Research Article

Dyeing sludge-derived biochar for efficient removal of malachite green from dyeing wastewater

Wei Qian[#], Yili Deng[#], Yongzheng Zhang, Yingying Li, Yi Fang, Xiaolong Li, Jialin Liang, Hui Liu

Department of College of Resources and Environment, Zhongkai University of Agriculture and Engineering, Guangzhou 510225, Guangdong, China.
[#]Authors contributed equally.

Correspondence to: Dr. Jialin Liang, Prof. Hui Liu, Department of College of Resources and Environment, Zhongkai University of Agriculture and Engineering, No. 501 Zhongkai Road, Haizhu District, Guangzhou 510225, Guangdong, China. E-mail: jialin.liang@zhku.edu.cn; liuhui@zhku.edu.cn

Abstract

In light of the rapid advancement of the dyeing industry, the resultant environmental contamination from extensive dye utilization and the subsequent sludge generated by the treatment of dyeing wastewater has escalated, prompting broad apprehension. This study employed the response surface methodology to explore the iodine adsorption capacity of pyrolyzed dyeing sludge peat treated with $ZnCl_2$ [$ZnCl_2$ modified sludge biochar (ZSC)] as the adsorbent material for optimization of the parameters for ZSC preparation. The analysis of the variance of the response surface methods indicated that the pyrolysis temperature emerged as the most pivotal factor. The maximum adsorption capacity of malachite green (MG) by ZSC reached up to 224.0962 mg/g. Moreover, the adsorptive efficacy of ZSC on MG was evaluated under varying environmental conditions, showcasing that the optimal parameters facilitated a remarkable MG removal efficiency of 99.13%. Even after five cycles of reuse, ZSC maintained a substantial decolorization capability of 45% for MG. Characterization of ZSC through scanning electron microscopy (SEM), X-ray diffraction (XRD), Fourier transform infrared spectroscopy (FT-IR), and Brunauer–Emmett–Teller (BET) indicated a high specific surface area of 495.38 m^2/g and the presence of reactive functional groups (–OH and C–O). The adsorption process, upon thermodynamic and kinetic evaluation, aligned more closely with the Langmuir isotherm model and the pseudo-second-order kinetic model. Mechanistic adsorption results revealed that electrostatic attraction, pore-filling, hydrogen bonding, and π-π stacking

interactions collectively accounted for the elevated MG removal efficacy by the ZSC. This study represents a promising approach, transforming waste into a treatment solution with the dual purpose of dye removal and resource reclamation from dyeing sludge.

Keywords: Dyeing sludge biochar, adsorption mechanism, malachite green removal, dyeing wastewater

INTRODUCTION

With the swift evolution of the industry, the scourge of textile wastewater contamination is escalating. In China, the annual discharge of textile wastewater amounts to approximately 2.0-2.3 billion tons, representing 11% of the nationwide total wastewater release. Dyeing, the pivotal contributor within the textile industry, generates a large amount of dyeing wastewater daily (300-400 × 10⁴ tons), which constitutes 70%-80% of the total effluent in the industry[1,2]. Dyes, extensively employed in textile dyeing, served as the primary source of pollutants in dyeing effluents, engendering wastewater with intense coloration, salinity, heightened organic matter concentration, and intricate compositions[3]. Notably, malachite green (MG) is a dye that also functions as a fungicide, bactericide and parasiticide, characterized by persistence and resistance to natural decomposition. Previous studies have shown that MG possesses a residual period of up to 44 and 342 days in two species of fish, Oreochromis niloticus and Piaractus mesopotamicus, thus posing a significant threat to ecosystems and human well-being[4-6]. Currently, physical and biological treatments[7-11] are predominantly utilized for the remediation of dyeing wastewater; however, substantial sludge would yield and then trigger secondary pollution. Therefore, adsorption treatment has emerged as a widely approved approach due to its efficacy and cost-effectiveness in the removal of dyes from wastewater.

At present, countless endeavors have been dedicated to the development of potent and economical adsorbents for the removal of dyes. Xue *et al.* and He et al. utilized magnetic adsorbents and activated carbon materials for treating dyes, with superior adsorption performance[12,13]. The selection of an adsorbent is paramount in influencing the efficacy of adsorption, with its specific surface area and active sites deemed critical structural and compositional attributes that exert a substantial influence on adsorption phenomena[14]. Presently, carbon-based materials, including biochar and carbon nanotubes, were predominantly acknowledged as adsorbents for extensive application in the decolorization of dye-laden wastewaters, which was attributed to their abundant porous structure, active sites, and elevated specific surface area[15,16]. Notably, biochar, derived from a diverse range of feedstocks, like sludge, lignin-rich biomass, and spent mushroom substrate, has garnered significant interest in the remediation of dyeing-contaminated wastewater because of its exceptional efficacy. For example, Boulanger *et al.* prepared activated carbon for adsorption of activated orange 16 using waste mushroom substrate and virgin birch wood, respectively, and the maximum adsorption was more than 500 mg/g in both cases[17-19]. The advancement and upscaling of biochar application in water purification processes are imperative to foster sustainable practices in wastewater treatment.

In recent years, China has witnessed a dramatic escalation in dyeing sludge output, with the dyeing industry generating ~2.3 million tons of toxic and hazardous dyeing sludge in 2020[20]. Dyeing sludge often comprises polycyclic aromatic hydrocarbons (PAHs), heavy metals, surfactants, dyes, solvents, and detergent compounds. Conventional sludge management strategies like landfilling, incineration, and composting scarcely align with environmental stewardship, particularly concerning dyeing sludge. For example, landfilling of dyeing sludge may pose a risk to the environment as hard-to-degrade pollutants accumulate in the sludge and result in a loss of opportunity to convert the sludge into a resource. Incineration of sludge allows for thermal or electrical energy reduction and energy recovery, but the potential flue gas emissions

carry a high environmental risk. Composting of sludge needs to ensure that toxic substances in dye sludge are effectively degraded or controlled during the composting process to avoid contamination of soil and water bodies. Nonetheless, the rich organic content of dyeing sludge offers potential for resource recovery through thermochemical conversion processes[21]. The transformation of sludge into biochar via pyrolysis emerged as a win-win solution that not only reduced sludge volume but also promoted material reclamation. Gong *et al.* utilized life cycle assessments to evaluate the potential of dyeing sludge biochar[20]. Results indicated that the sludge biochar was the most favorable choice for the transformation of dyeing sludge treatment technology due to its low direct pollutant emissions and its ability to replace high-value products. Moreover, pyrolytic carbonization of dyeing sludge promoted the immobilization of heavy metals in the biomass, which reduced the bioavailability and mobility of heavy metals[22]. Although the carbonized dyeing sludge via pyrolysis presented a promising avenue for dyeing sludge treatment, the elevated ash content and diminished organic matter content led to a reduced specific surface area and substandard surface functional group properties, thereby impeding its further utilization[23,24]. To enhance its properties, chemical activation techniques, especially those employing agents like KOH, $ZnCl_2$, H_2SO_4, *etc.*, were increasingly favored[25-30]. Among them, $ZnCl_2$ served as an exemplary activating agent in the preparation of biochar, owing to its ability to transform the material into one with expansive surface areas and finely-tuned pore structure[31]. In this regard, utilizing $ZnCl_2$ could probably enhance the performance of the biochar materials derived from dyeing sludge. Nonetheless, scant research has been dedicated to the fabrication of high-efficacy adsorbent materials targeting dye MG from dyeing sludge waste modified by $ZnCl_2$. The influence of the activation methodology and the pyrolysis process on adsorption efficacy have yet to be comprehensively investigated. Moreover, the underlying adsorption mechanisms warrant a more profound understanding.

Hence, this study employed dyeing sludge as the primary ingredient and $ZnCl_2$ solution as an activator for the synthesis of high-performance adsorbents through pyrolysis. First, the optimization of pyrolysis conditions (pyrolysis temperature, activation ratio, and carbonization duration) on the production of pyrolyzed dyeing sludge treated with $ZnCl_2$ [$ZnCl_2$ modified sludge biochar (ZSC)] was conducted. Second, the adsorption of MG from dyeing wastewater involved a thorough examination of variables such as adsorption equilibrium time, initial pH, initial MG concentration, ZSC dosage, and adsorption temperature, in order to ascertain the favorable conditions for adsorption. Third, the stability of the adsorbent materials was evaluated. Fourth, thermodynamic and kinetic models were used to elucidate the adsorption characteristics of MG in wastewater, shedding light on the underlying mechanism of its adsorption by the ZSC.

MATERIALS AND METHODS
Experimental materials
The dyeing sludge was taken from a dyeing sewage treatment plant in Foshan, Guangdong. I_2, $Na_2S_2O_3$, KIO_3, and $ZnCl_2$ were purchased from Fuchen Chemical Reagent Co. Ltd (Tianjin, China) and MG was obtained from Shandong Yousuo Chemical Technology Co. Ltd (Shandong, China). All chemicals used in the experiments were of analytical grade. The standard solution of MG was prepared with ultrapure water and diluted with distilled water.

Preparation of ZSC
The dyeing sludge was conserved post-drying and crushing. A specific quantity of dried sludge was blended with a $ZnCl_2$ solution (3 mol/L) at a designated mass ratio (ratio of solution to sludge was 1:2, 2:1, and 1:1), and allowed to permeate for 24 h at ambient temperature. Subsequently, the samples were filtered, dried in an oven at 105 °C until attaining a constant mass, and sealed for storage. The sludge samples were placed in a tube-type resistance furnace and heated up to the setting temperature (700-900 °C) at a rate of 10 °C/min

and remained for a certain period (1-2 h), and then taken out once the temperature had returned to ambient conditions, thereby obtaining sludge biochar under different preparation conditions. The samples were subjected to an acidification process using a 5% solution of hydrochloric acid to remove soluble ash on the surface of the biochar. Afterwards, the samples were rinsed with water, and subsequently dried to obtain the ZSC, and then sealed for storage.

Adsorption experiment

Simulated wastewater was prepared using MG as the treatment object, and all the experimental operations requiring pH adjustment were carried out using 0.1 M HCl and NaOH[32]. In this experiment, the effects of various influencing factors on the adsorption experiments were considered. The pH of the stock solution was maintained, and the adsorption equilibrium time of ZSC on MG was investigated at a certain concentration and ZSC dosage. The effect of initial pH on adsorption efficiency was investigated at the initial pH range of 2.0-10.0. The effect of initial MG concentration on adsorption experiments was investigated at six different concentrations of MG solution (150-400 mg/L). Seven different ZSC dosages (0.8-5.0 g/L) were used to investigate the effect of ZSC dosage on adsorption. Three temperatures (20, 30, and 40 °C) were used to study the adsorption of MG at different times. Furthermore, the adsorption removal of MG by ZSC was examined after five times of reuse. Comparative tests were conducted using unmodified sludge biochar (SC). Each test was carried out in triplicate.

Characterization

The concentration of MG in the solution was determined using a UV-Vis spectrophotometer at 630 nm (UV-1600-PC, Shanghai, China). The microscopic morphology of ZSC was observed by scanning electron microscopy (SEM, Helios-G4-CX, Thermo Scientific, US). The physical phase of ZSC was analyzed by X-ray diffraction (XRD, D8, Bruker, US). The atomic structure and functional groups of ZSC were analyzed by Fourier transform infrared spectroscopy (FT-IR, Nicolet 6700, Thermo Scientific, US). Nitrogen adsorption/desorption curves were determined by an automated gas sorption analyzer (Autosorb-iQ-MP, Quantachrome, US). The pore structure and other parameters of ZSC were calculated and analyzed using the Brunauer–Emmett–Teller (BET) method.

Analytical methods

A Box-Behnken design (BBD) within the response surface methodology (RSM) was employed to optimize the ZSC adsorption processes, aiming for efficacious iodine adsorption value. The iodine adsorption value was measured using the standard method. The optimal levels were determined from the experiments, and their calculation formulas were as follows [Equations (1-3)]:

$$A = \frac{X}{M}D \tag{1}$$

$$\frac{X}{M} = \frac{5(10c_1 - 1.2c_2V_2) \times 126.93}{m} \tag{2}$$

$$c = \frac{c_2V_2}{10} \tag{3}$$

Where A is the iodine adsorption value of the specimen, mg/g; X/M is the amount of iodine adsorbed per gram of activated carbon, mg/g; D is the correction factor; c_1 is the concentration of the iodine ($1/2\ I_2$) standard solution, mol/L; c_2 is the concentration of the sodium thiosulfate standard solution, mol/L; V_2 is the volume of the sodium thiosulfate standard solution consumed, mL; M is the mass of the specimen, g.

The adsorption removal rate of MG solution was calculated by Equation (4):

$$\text{Adsorption removal (\%)} = \frac{(c_0 - c_t)}{c_0} \times 100\% \tag{4}$$

Where c_0 is the initial concentration of simulated wastewater, mg/L; c_t is the concentration of simulated wastewater after adsorption and decolorization by ZSC, mg/L.

In this paper, Langmuir adsorption isotherm and Freundlich adsorption isotherm were used to fit the adsorption data of MG, respectively. Langmuir and Freundlich's adsorption isotherm expressivity were shown in Equations (5) and (6):

$$\frac{C_e}{q_e} = \frac{1}{q_m}C_e + \frac{1}{K_l q_m} \tag{5}$$

$$\ln q_e = \ln K_f + \ln C_e \frac{1}{n} \tag{6}$$

Where q_e is the amount of adsorbed mass per unit of adsorbent at adsorption equilibrium, mg/g; q_m is the maximum adsorbed mass that can be adsorbed by the monomolecular layer on the surface of the adsorbent during the adsorption process, mg/g; C_e is the concentration of the solute in the equilibrium liquid phase during the adsorption process, mg/L; K_l is the Langmuir adsorption coefficient; K_f is the Freundlich adsorption coefficient; n is the concentration index.

For adsorption kinetic analysis, Lagergren's pseudo-first and pseudo-second adsorption kinetic model and Elovich model were used in this paper. The equations are shown in Equations (7-9):

$$\ln(q_e - q_t) = \ln q_e - k_1 \tag{7}$$

$$\frac{t}{q_t} = \frac{1}{k_2 q_e^2} + \frac{t}{q_e} \tag{8}$$

$$q_t = \frac{1}{\beta}\ln(\alpha\beta) + \frac{1}{\beta}\ln t \tag{9}$$

Where q_e is the amount of adsorbate on the unit adsorbent at adsorption equilibrium, mg/g; q_t is the amount of adsorbate on the unit adsorbent at the moment of t, mg/g; t is the time, min; k_1 is the adsorption rate constant of the pseudo-first kinetic adsorption model; k_2 is the adsorption rate constant of the pseudo-second kinetic adsorption model; α (mg/g/min) is the initial adsorption coefficient; β (g/mg) is the desorption coefficient.

RESULTS AND DISCUSSION
### Optimization of pyrolysis conditions
In the RSM study, three factors including pyrolysis temperature (A), carbonization time (B), and activation ratio (C) were used as independent variables, and ZSC iodine adsorption amount was chosen as the response value (Y). The specific experimental factors and levels are shown in Supplementary Table 1. The experimental results are shown in Table 1. The results were regressed using Design Expert 12 software to establish the quadratic regression equation between iodine adsorption amount and the three single factors (pyrolysis temperature, pyrolysis time, and activation ratio). The analysis of variance (ANOVA) of the regression equations is shown in Supplementary Table 2. From the data in Supplementary Table 2, the model F-value was 22.66 and the *P*-value was 0.0002, indicating that the model could well optimize the

Table 1. Experimental design scheme and results

No.	Factor			Iodine adsorption capacity (mg/g)
	Pyrolysis temperature (°C)	Carbonization time (h)	Activation ratio	
1	700	1	1.25	274.16
2	900	1	1.25	289.55
3	700	2	1.25	296.92
4	900	2	1.25	285.2
5	700	1.5	0.5	300.91
6	900	1.5	0.5	303.47
7	700	1.5	2	318.35
8	900	1.5	2	320.66
9	800	1	0.5	300.67
10	800	2	0.5	285.75
11	800	1	2	304.53
12	800	2	2	320.19
13	800	1.5	1.25	324.53
14	800	1.5	1.25	335.21
15	800	1.5	1.25	340.99
16	800	1.5	1.25	339.58
17	800	1.5	1.25	338.79

preparation of biochar from dyeing sludge.

The response surface plots of the interaction effects of the different factors on iodine adsorption were shown in Figure 1. According to the model fitting, it could be obtained that the significance of the three factors was in the order of pyrolysis temperature > activation ratio > carbonization time. The quadratic terms A^2, B^2, and C^2 were all significant for the model ($P < 0.05$), and the interactions of the three factors were non-significant ($P > 0.05$). Figure 1A, C and E showed the interaction of all variables on iodine adsorption. As shown in Figure 1A, when the modification ratio was fixed, both calcination temperature and calcination time would affect iodine adsorption. Increasing calcination temperature could significantly increase iodine adsorption capacity, and the highest point of iodine adsorption appears at a calcination temperature of 800-850 °C for 1.4-1.7 h. As shown in Figure 1C, when the pyrolysis time was fixed, both temperature and modification ratio would affect iodine adsorption. At the same time, at lower temperatures, the iodine adsorption capacity was low, and the improvement of iodine adsorption capacity by modification ratio was not obvious, which meant that the iodine adsorption capacity could be improved at higher temperatures, and the highest point of iodine adsorption appears at 800-850 °C, and the modification ratio was between 1:1 and 2:1. The iodine adsorption of these two figures increased with rising pyrolysis temperatures, and the response surface inclination became more obvious. This suggested that the temperature elevation induced the dissociation of alkyl groups and a subsequent rise in aromaticity within the ZSC[33], thereby facilitating the formation of a porous framework and enhancing the adsorptive capacity. As shown in Figure 1E, when the temperature was fixed, both pyrolysis time and modification ratio would affect iodine adsorption, but the curvature of the surface depicted in Figure 1E was minimal and their impact on the quantity of iodine adsorbed was nearly equivalent. The peak time of iodine adsorption is 1.4-1.7 h, and the modification ratio was 1:1-2:1. As shown in Figure 1B, D and F, we could see that the interaction between the two experimental factors had a significant impact on the response variables. The contour lines in Figure 1B and D were elliptical, indicating that there was an obvious interaction between pyrolysis temperature and pyrolysis time, and between pyrolysis temperature and modification ratio. The contour lines in Figure 1F were close to a circle, indicating that the interaction between pyrolysis time and
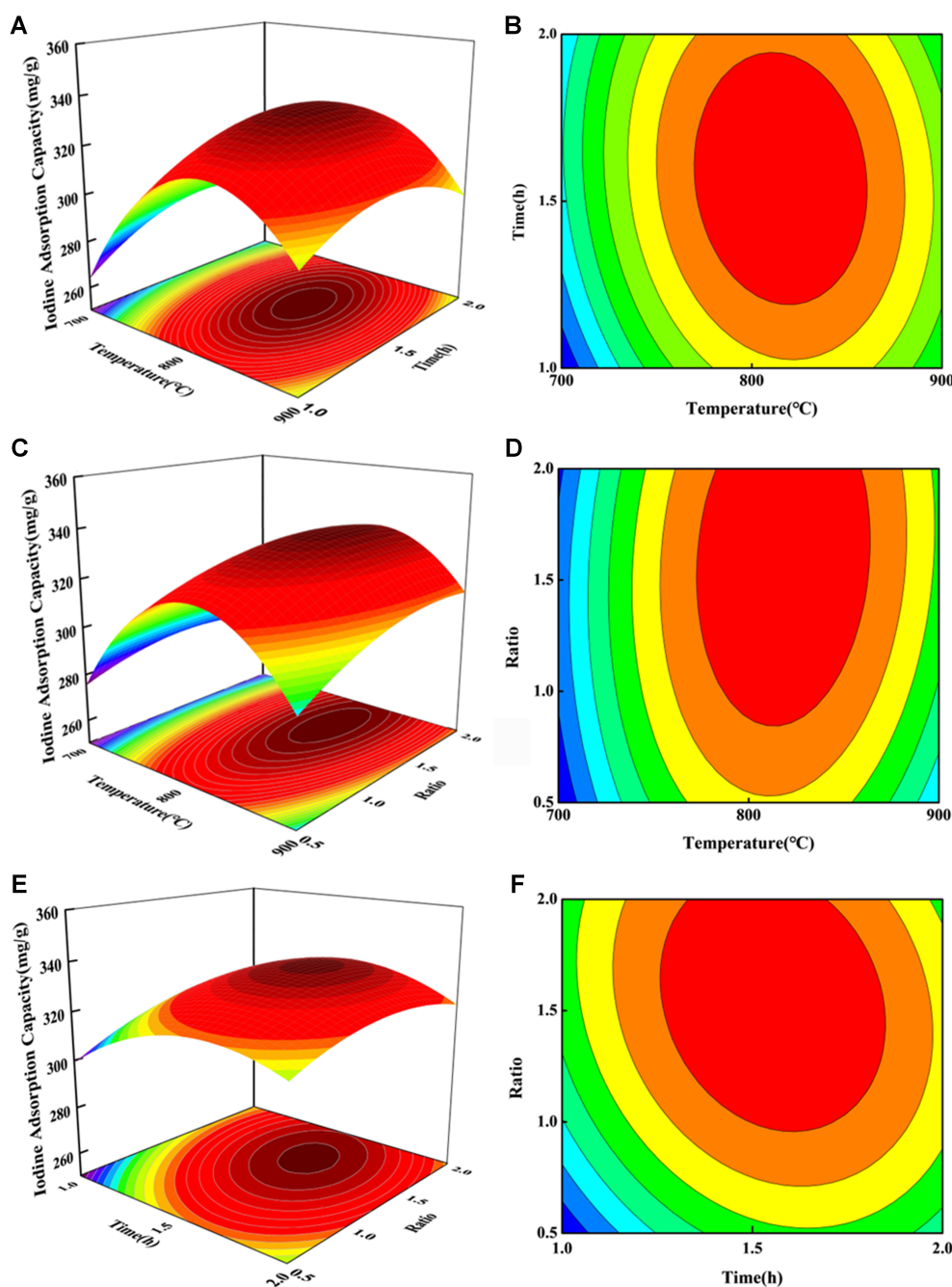
Figure 1. Response surfaces and contours of iodine adsorption by ZSC under three single factors. (A) Three-dimensional response surfaces and (B) contour plots of pyrolysis temperature (700-900 °C) *vs.* pyrolysis time (1.0-2.0 h); (C) Three-dimensional response surfaces and (D) contour plots of pyrolysis temperature (700-900 °C) *vs.* mass ratio of $ZnCl_2$ to sludge (1:2-2:1); (E) Three-dimensional response surfaces and (F) contour plots of pyrolysis time (1.0-2.0 h) *vs.* mass ratio of $ZnCl_2$ to sludge (1:2-2:1). ZSC: $ZnCl_2$ modified sludge biochar.

modification ratio was not significant. Based on the RSM results, the quadratic models for optimization of ZSC preparation were shown in Equation (10). From the model, the optimal preparation process of ZSC from dyeing sludge was selected as an activation temperature of 800 °C, an activation ratio of 1:1, and a carbonization time of 1.5 h. Under such conditions, the predicted iodine adsorption value in the model was 336.63 mg/g. In order to further validate the discrepancy between experimental and model-predicted values,

validation experiments were carried out under the above conditions. The corresponding iodine adsorption value was 341.05 ± 1.31 mg/g, confirming the accuracy of this model. In summary, the pyrolysis temperature had the most significant effect on iodine adsorption, followed by the activation ratio and the carbonization time, which was similar to the experimental results obtained by Liang *et al.*[34].

$$Y = -2348.465 + 6.066A + 248.888B + 17.728C - 0.086AB + 0.049AC - 9.613BC - 0.004A^2 - 53.298B^2 - 13.661C^2 \quad (10)$$

Where Y is the iodine adsorption amount, mg/g; A, B, and C are the pyrolysis temperature, carbonization time, and the ratio of immersion activation, respectively.

Characterization of ZSC and SC

The surface morphology of ZSC ($ZnCl_2$ modified sludge biochar) and SC is shown in Figure 2A and B. The SC surface exhibited a sleek texture with minimal pore structure, while the ZSC obtained after $ZnCl_2$ activation showcased a rough and non-uniform surface composition adorned with aggregated fine particles adhering to its surface, alongside a more intricate pore arrangement. This observation was confirmed by the BET surface area [Table 2]. This was probably due to the fact that the $ZnCl_2$ activator promoted water release at higher temperatures (610 °C), leading to the expansion and unsealing of the sludge pores as zinc vapors and various gases were discharged. Accordingly, this process augmented the porosity of the ZSC[35]. Meanwhile, the presence of $ZnCl_2$ could accelerate the fragmentation of the organic matter in the sludge, consequently promoting the pore space in ZSC and enhancing the specific surface area of ZSC[31,36]. Meanwhile, the pore diameter and porosity of ZSC were also enhanced after the acid treatment to remove the metal oxide particles and ash on the surface[37].

The XRD patterns of the sludge biochar before and after modification are shown in Figure 2C. The diffraction patterns of the two sludge biochars exhibited a fundamental similarity involving a range of mineral constituents (such as silicon, calcium, *etc.*). However, the intensity of the diffraction peaks of ZSC surpassed that of SC at certain angles. A large number of diffraction peaks of SC were observed, notably at 2θ = 20.95°, 26.72°, and 50.22°, corresponding to the crystal surface reflections of SiO_2 (100), (011), and (112), respectively. Additionally, a peak at 26.65° corresponded to the reflection of graphitic carbon (002) crystals, while a distinct peak at 29.49° indicated the presence of $CaCO_3$, potentially attributed to the large amount of metal content within the sludge. After the modification with $ZnCl_2$, ZSC displayed distinct diffraction peaks, notably with enhanced intensity 2θ = 20° and 26° compared to SC. Moreover, the narrow and sharply defined range of these peaks suggested an improved crystal structure and heightened crystallinity within ZSC. The weak diffraction peak at 2θ = 45° corresponded to the crystalline reflection of graphitic carbon (100), implying that the prepared sample could potentially be a carbon-based material due to the accumulation of irregular aromatic layer structure[25,38].

As shown in Figure 2D, each band in the FT-IR spectra represented the vibration of functional groups in the ZSC and SC. The peaks of the two sludge carbon spectra appeared at basically similar wavelengths but with slightly different intensities. Such differences between ZSC and SC might be attributed to the various contents of surface functional groups. A broad and short peak appeared at a wavelength of 3,400 cm^{-1} (-OH expansion and contraction vibration) in the ZSC and SC samples, indicating that hydroxyl and carboxyl groups existed in both ZSC and SC. The spectral band at 2,923 cm^{-1} correlated with the aliphatic $-CH_3$ stretching vibration; however, this vibration presented as subdued, potentially attributable to the decomposition of aliphatic C–H bonds into gaseous byproducts like CO_2 and CH_4, or their conversion into aromatic configurations under high-temperature conditions, culminating in less pronounced absorption

Table 2. Pore structure characteristics of ZSC and SC

Dyeing sludge-derived biochar	Microporous specific surface area (cm^2/g)	Specific surface area (cm^2/g)	Pore volume (cm^3/g)	Total pore volume (cm^3/g)	Average pore diameter (nm)
ZSC	58.219	495.38	0.054	0.458	3.703
SC	42.227	359.78	0.039	0.333	3.698

ZSC: $ZnCl_2$ modified sludge biochar; SC: unmodified sludge biochar.
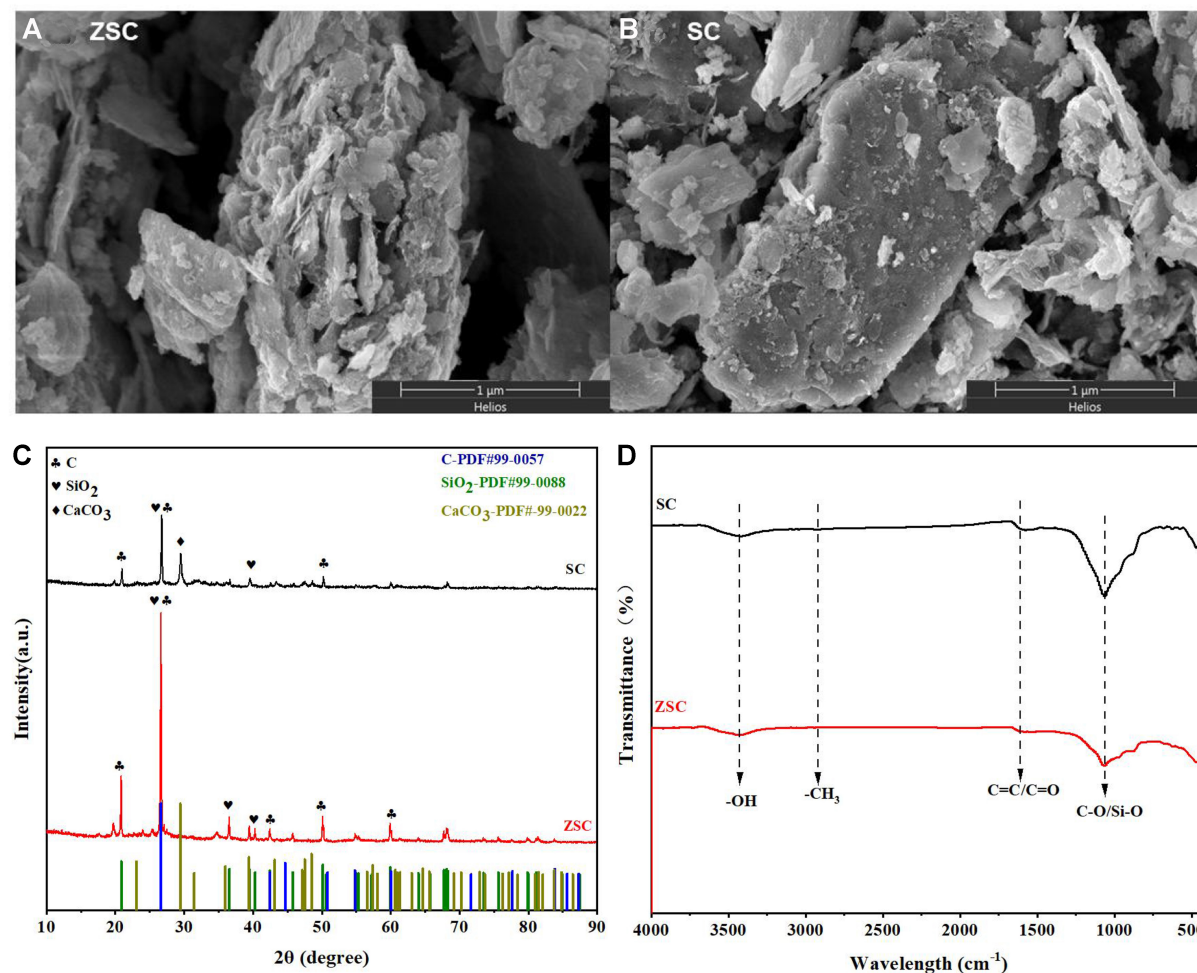
Figure 2. SEM images of (A) ZSC (B) and SC; (C) XRD pattern of ZSC and SC; and (D) FT-IR of ZSC and SC. SEM: Scanning electron microscopy; ZSC: $ZnCl_2$ modified sludge biochar; SC: unmodified sludge biochar; XRD: X-ray diffraction; FT-IR: Fourier transform infrared spectroscopy.

peaks[33]. The corresponding absorption peak at 1,650 cm^{-1} was attributed to the stretching vibration of C=C in the aromatic ring. The weak peaks at 800-1,100 cm^{-1} might be attributed to the stretching vibrations of functional groups such as C–H and C–O–C[39,40]. In addition, two sharp and wide absorption peaks appeared at 1,050 and 800 cm^{-1}, which corresponded to the stretching vibrations of C–O/Si–O and Si–O, respectively[35]. It should be noted that the strengths of functional groups in ZSC, especially in oxygen-containing groups, are weaker than those of SC. During the activation phase, $ZnCl_2$ was capable of engaging not merely with carbon, but also with the oxygen and hydrogen constituents of the biochar[30], attenuating the prominence of these characteristic peaks. This interaction was conjectured to promote the establishment

of hydrogen bonds among the nitrogen and oxygen-containing groups on the contaminants.

The pore structure parameters as well as adsorption isotherms and pore size distribution curves of ZSC and SC derived from BET and Barrett-Joyner-Halenda (BJH) methods were shown in Table 2 and Figure 3. As present in Table 2, the specific surface area of ZSC and SC was higher than 350 cm^2/g, while the pore volume was higher than 0.03 cm^3/g. This result indicated high specific surface area and large pore volume in ZSC and SC, which facilitated the efficient and efficacious adsorption of dye, resulting in a markedly superior adsorptive performance[41]. Noticeably, the specific surface area and pore volume of ZSC were > 1.37-fold compared to those of SC, suggesting superior pore structure characteristics in ZSC. This pore structure contributes to better adsorption performance. As could be seen from Figure 3A and C, the adsorption-desorption isothermal curves of ZSC and SC belong to type IV isotherms with H$_4$ hysteresis loops in the IUPAC classification method, indicating that mesoporous structures existed in both materials. The adsorption and desorption were parallel and nearly horizontal, which might be due to the capillary coalescence phenomenon under low pressure[35,42]. Figure 3B and D showed the pore size distribution of ZSC and SC. The average pore size distribution of ZSC and SC was between 3-120 nm, and both of them were predominantly concentrated in the range of 3-10 nm. This result suggested that the pore structure of both kinds of sludge biochar was predominantly mesoporous, with a small number of macropores present. The results showed that the pore structures of ZSC and SC were suitable for the adsorption of pollutants. Given that ZSC possessed a greater specific surface area, larger pore structure, and an abundance of surface functional groups, it likely exhibited an exceptional adsorptive capacity of MG.

Effect of different factors on MG adsorption

In this study, the effects of five factors on the adsorption process, namely, adsorption equilibrium time, initial MG concentration and initial pH of MG solution, ZSC dosage, and adsorption temperature, were considered, and the results were shown in Figure 4. As depicted in Figure 4A, the rate of decolorization gradually escalated with the extension of the duration of MG adsorption by ZSC, culminating in a heightened adsorption rate until reaching a state of equilibrium, where the pace of adsorption gradually decelerated. The decolorization efficacy surged from 0% to 71% within the initial 120 min, followed by a 2.33% increment in the decolorization efficiency of MG between 120 and 210 min. Accordingly, the adsorption of MG by ZSC showed swiftness within the first 120 min, transitioning gradually to a sluggish adsorption process as time progressed toward equilibrium[43].

The change in solution pH value affects the surface charge of the adsorbent. As such, in this study, the effect of pH in the range of 2-10 on the adsorption process was examined, and the results are shown in Figure 4B. With the increase in pH, the removal rate of MG by ZSC gradually elevated. Notably, the removal rate of MG at pH = 10 was as high as 99.7%, inferring that ZSC was more suitable for MG removal in an alkaline environment. This may be due to the fact that MG was a cationic dye with a positive charge in an aqueous solution and at a pH > 10; this pH level surpassed the zero-charge threshold of ZSC, prompting the deprotonation of the oxygenated functional groups in ZSC[2], thereby facilitating the adsorption of MG. In contrast, in an acidic environment with a lower pH, the anionic groups in ZSC bind with H$^+$ in the solution and diminish the number of anionic adsorption sites, leading to a lower adsorption rate[44]. Therefore, pH = 10 was selected as the optimal pH for the adsorption process.

Figure 4C reflected the effect of the initial concentration of MG solution on the adsorption process. With the increase in MG concentration, the removal rate of MG gradually decreased. When treating the MG solution with a concentration of 400 mg/L, the removal rate reached about 50%. The reduction of MG removal was due to the saturation of adsorption capacity in ZSC[45]. If treating a high concentration of dye
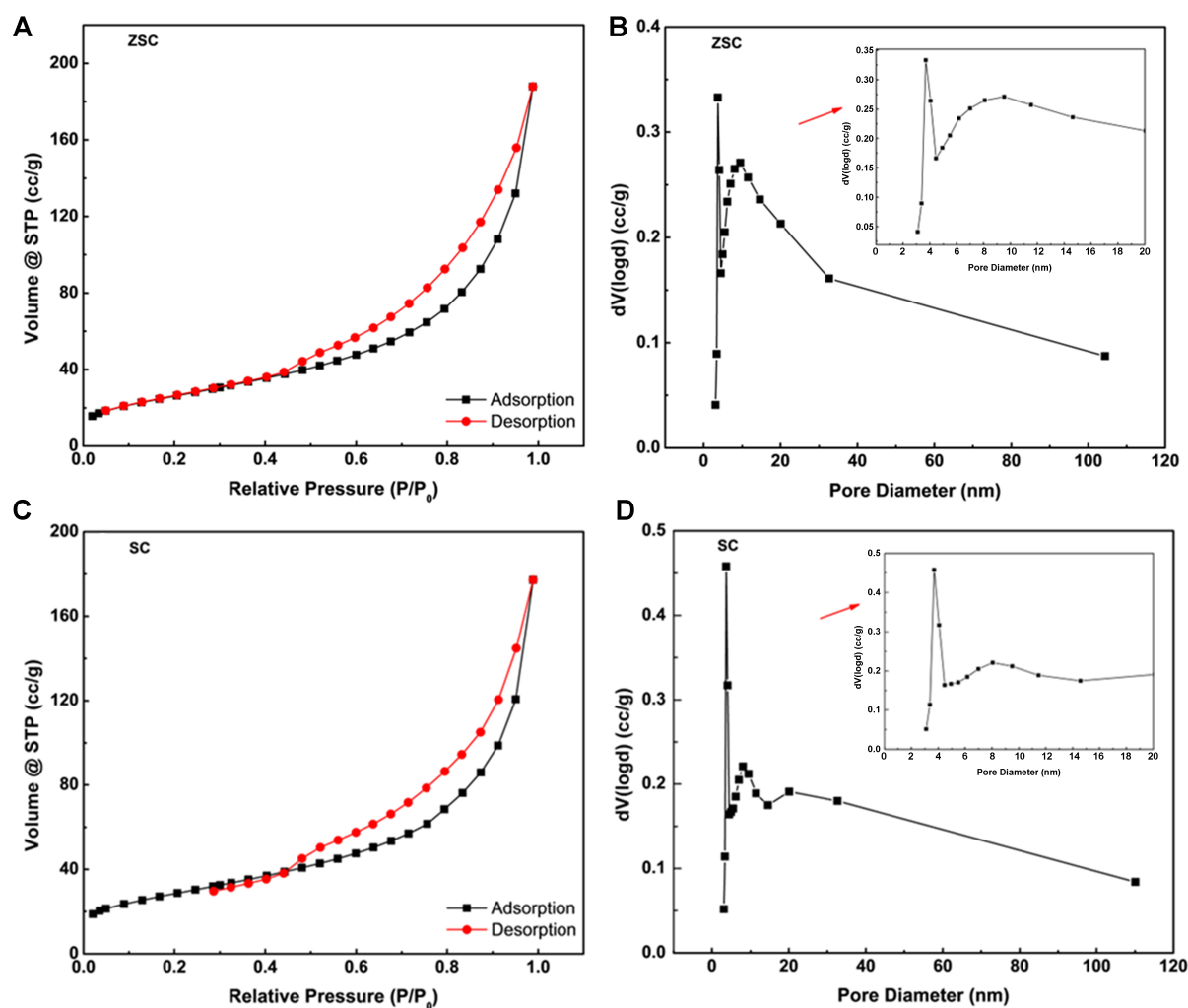
Figure 3. BET N_2-adsorption/desorption isotherm of (A and B) ZSC and (C and D) SC. BET: Brunauer–Emmett–Teller; ZSC: $ZnCl_2$ modified sludge biochar; SC: unmodified sludge biochar.

wastewater, it was necessary to dose more adsorbents in order to achieve a higher removal rate. In practice, the use of small quantities of adsorbents to treat high-concentration wastewater was unsatisfactory. Overall, a concentration of 150 mg/L was chosen as the optimum treatment concentration for the adsorption test.

Figure 4D examined the adsorption performance of MG with different ZSC dosages. The adsorption amount of MG exhibited a remarkable acceleration as the dosage of ZSC surged from 0.8 to 3.2 g/L. Correspondingly, the adsorption amount of MG increased from 79.44 to 261.30 mg/g. Further escalation of the dosage to 5 g/L slowly enhanced the adsorption amount to 298.38 mg/g, suggesting the saturation of adsorption process.

As shown in Figure 4E, temperature has a large influence on the adsorption process. Typically, the adsorption process tends to be inherently exothermic. Surprisingly, as the temperature rises during adsorption equilibrium, rather than a decline in adsorption capacity, there is an upward trend. This may be due to elevated temperatures fostering molecular diffusion, resulting in high adsorption capacity. Nonetheless, under lower temperatures, low adsorption capacity may be due to the influence of mass
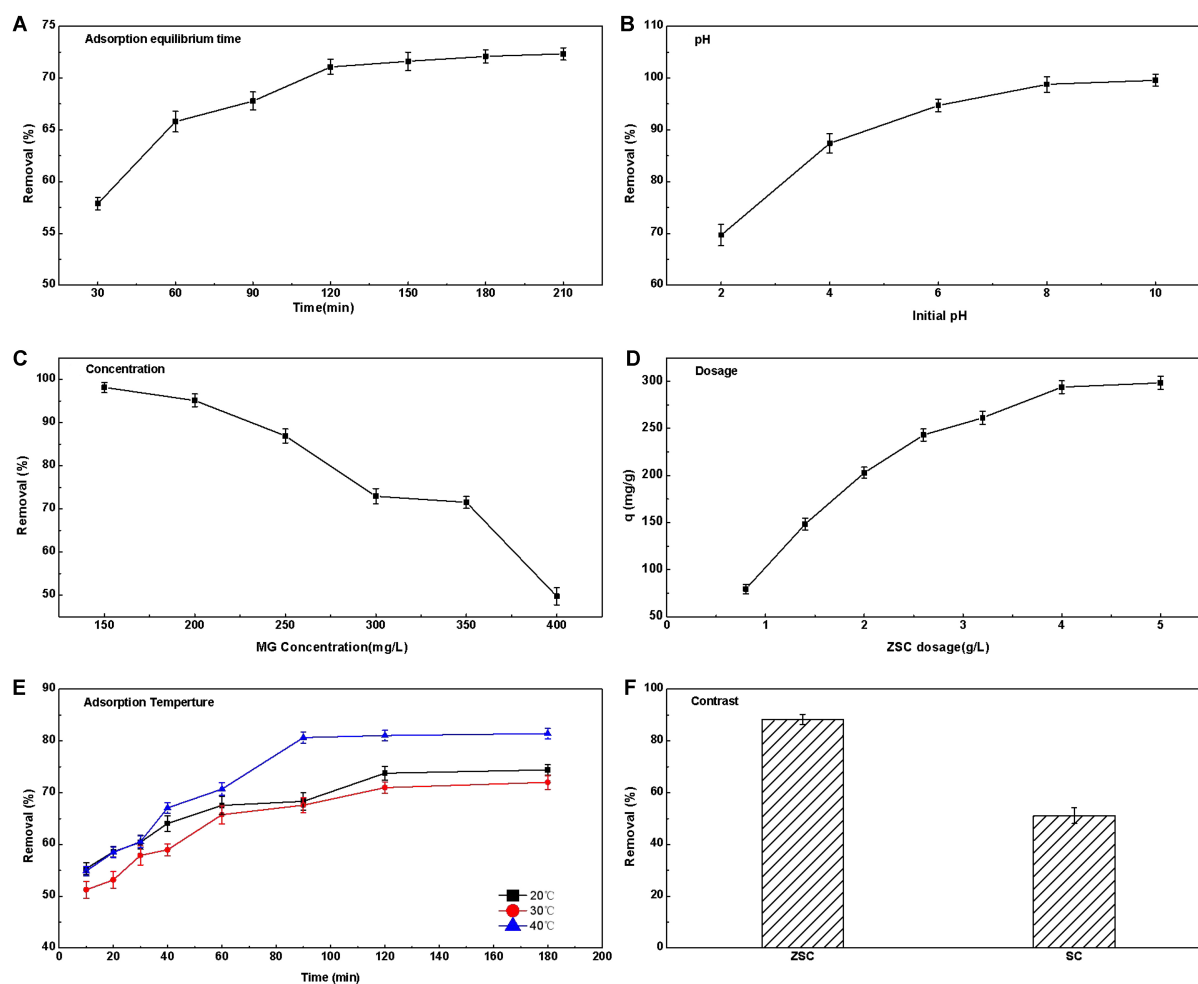
Figure 4. Impacts of different factors of ZSC on the MG adsorption. (A) Adsorption equilibrium time (operation condition: initial pH = stock solution, ZSC dosage = 2 g/L, MG concentration = 300 mg/L, and room temperature); (B) Initial pH of solution (operation condition: reaction time = 120 min, ZSC dosage = 2 g/L, MG concentration = 300 mg/L, and room temperature); (C) MG concentration (operation condition: initial pH = 10.0, reaction time = 120 min, ZSC dosage = 2 g/L, and room temperature); (D) ZSC dosage (operation condition: initial pH = 10.0, reaction time = 120 min, MG concentration = 150 mg/L, and room temperature); (E) Adsorption temperature (operation condition: initial pH = 10.0, reaction time = 120 min, ZSC dosage = 2 g/L, and MG concentration = 150 mg/L); and (F) Comparison results of MG removal rate by ZSC and SC. ZSC: ZnCl$_2$ modified sludge biochar; MG: malachite green; SC: unmodified sludge biochar.

transfer resistance and particle diffusion limiting the rate of adsorption[46,47]. Ebrahimian Pirbazari *et al.* reported an enhancement in adsorption capacity of 57 mg/g when increasing the temperature from 30 to 40 °C, which was attributed to the enhanced diffusion rate of the pollutant molecules in the external boundary layer and internal pores of the adsorbent particles[48]. To expedite the adsorption kinetics, it becomes imperative to elevate the temperature, thereby inducing a phenomenon where the adsorption quantity escalates[2,23]. When the adsorption temperature was 40 °C, the growth of the adsorption rate was obvious in the first 90 min, as indicated by the removal rate of 80.47%. The removal rate began to tend to equilibrium after 120 min. However, at 20 and 30 °C, the growth of the adsorption rate was slow, and the adsorption gradually tended to an equilibrium state after 180 min, as indicated by the MG removal of 75% or less. Therefore, the reaction temperature was selected to be 40 °C.
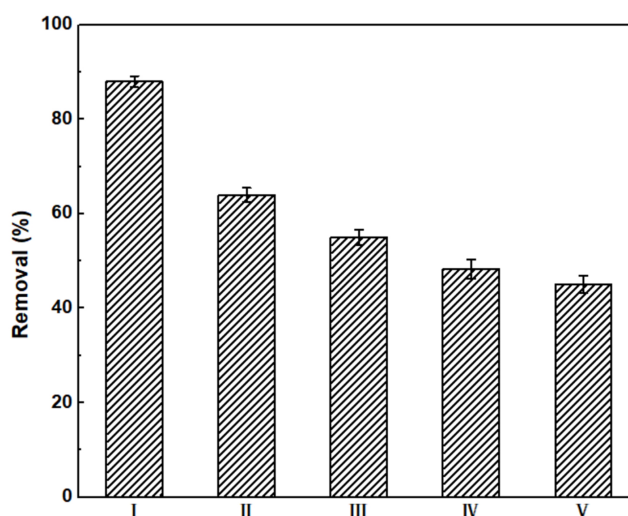
Figure 5. Reusability of ZSC as indicated by the MG removal. ZSC: ZnCl$_2$ modified sludge biochar; MG: malachite green.

In accordance with the above-mentioned results, the optimal conditions for MG removal were chosen as an initial pH of 10, an initial MG concentration of 150 mg/L, a ZSC dosage of 5 g/L, a reaction time of 120 min, and a temperature of 40 °C. Under such conditions, the removal rate of MG was as high as 99.13%.

In order to investigate the adsorption and decolorization effect of ZSC and SC on MG, the removal rate of MG was determined under the same conditions, and the results are shown in Figure 4F. The results showed that the removal rate of MG by ZSC was 37% higher than that of SC under the same conditions, which indicated that the activated sludge biochar had better adsorption performance. Employing dyeing sludge as an adsorbent enhanced the value proposition of sludge utilization, facilitating a more resourceful and sustainable approach to its utilization.

Reusability performance and comparative results of different sludge-derived biochar
In order to evaluate the durability and reusability of the ZSC system, a sequence of five-cycle tests was carried out for MG removal. The results of the adsorption performance of ZSC on MG after reusing were shown in Figure 5. The removal rate of MG by ZSC was close to 90% in the first round, while it was found that the removal rate of MG by ZSC was still around 50% after five cycles. It could be seen that the reusability of sludge-activated carbon was relatively high and could be reused to treat low-concentration dyeing in wastewater.

A comparative analysis of the adsorption efficacy of various sludge-derived biochar materials is presented in Table 3. The adsorption capacities of the modified carbon materials were 2.6-13.1 times higher than those of the unmodified ones, suggesting that chemical modification can promote pore formation and improve the adsorption performance of the materials. In addition, the dyeing sludge-derived biochar activated with ZnCl$_2$ in this study exhibited superior adsorption capabilities and specific surface areas, surpassing the performance of most previously documented adsorbents[49-53]. Unlike other adsorbents necessitating intricate production processes, severe operational conditions, or frequent replacements, this particular biochar can withstand complex conditions and demonstrate practical utility. With an adsorption capacity of 341.0 mg/g and a specific surface area of 495.4 m^2/g, this ZSC biochar exhibited excellent adsorption performance of MG.

Table 3. Comparison of different sludge-derived biochars and their adsorption properties on dyes

| Adsorbents	Activating agent	Dye	S_{BET} (m²/g)	Adsorption capacity (mg/g)	Ref.
Yarn sludge-derived biochar	KI/KOH	MG	1,037.0	498.0	[46]
Sewage sludge-derived biochar	Acetone	MG	17.0	38.6	[47]
Sewage sludge/waterworks sludge-derived biochar	/	Methylene blue	45.5	186.0	[48]
Sewage sludge-derived biochar	/	Remazol brilliant blue R	12.4	87.0	[49]
Sewage sludge/lignin-derived biochar	/	Methylene blue	33.6	38.1	[50]
Dyeing sludge-derived biochar	$ZnCl_2$	MG	495.4	341.0	This study

BET: Brunauer–Emmett–Teller; MG: malachite green.

Adsorption mechanism

Adsorption thermodynamic study

In Supplementary Table 3, it could be seen that the R^2 value of Langmuir isotherm (0.6819) was higher than that of Freundlich isotherm (0.4276), indicating the adsorption behavior of ZSC on MG probably conformed to the Langmuir isotherm. The maximum adsorption of MG by ZSC was 224.0962 mg/g, suggesting that the adsorption of MG occurring at ZSC was monomolecular layer adsorption.

Adsorption kinetic study

Adsorption temperature is a key factor in the removal of pollutants from water by adsorbents[20]. To further evaluate the adsorption kinetic behavior at different temperatures, quasi-primary and quasi-secondary models were used to fit the adsorption curves. Figure 6 and Supplementary Tables 4 and 5 reflected the relevant parameters of adsorption kinetics. In Supplementary Table 4, the maximum adsorption capacity in the pseudo-first model was 35.8234, 43.1939, and 48.9892 mg/g, respectively, at 20, 30, and 40 °C. Correspondingly, in Supplementary Table 5, the largest adsorption capacity at 20, 30, and 40 °C in the pseudo-second model was 114.9425, 112.3596, and 129.8701 mg/g, respectively. Notably, the maximum adsorption capacity in the pseudo-second model was remarkably higher than that of the pseudo-first model. The Elovich model is commonly used to describe the adsorption and desorption processes of chemisorption on non-uniform surfaces, and the results are shown in Figure 6D and Supplementary Table 6. The correlation coefficients indicated that the adsorption process fits well with the Elovich model, and in this experiment, the adsorption rate was much larger than the desorption rate[54]. Furthermore, by comparing the R^2 values of the pseudo-first, pseudo-second kinetic equations and Elovich equations, it was found that the linear correlation coefficient of the pseudo-second kinetic model was closer to 1. Therefore, the process of MG adsorption by ZSC was more suitable to be described by the pseudo-second kinetic model. In addition, this paper further used the intra-particle diffusion model to fit the data on the adsorption capacity of the wastewater treated by the material with time, and the results are shown in Figure 6E and Supplementary Table 7. By segmenting the fitted curves, it was believed that the adsorption process could be roughly divided into two stages: the surface mass transfer stage and the intra-particle diffusion process. By comparing the values of K_d in the different stages, the value of K_{d2} was found to be the smallest in the second stage, which indicated that the rate of the intra-particle diffusion process slowed down until the adsorption rate decreased. Then, the rate of the process slows down until the adsorption is saturated. Meanwhile, the adsorption capacity q_t of the material showed a good linear relationship with $t^{1/2}$, but did not pass through the origin, indicating that the internal diffusion is not the only rapid control step of the adsorption process[55,56]. Based on the above results, it is illustrated that the overall adsorption reaction rate is controlled by the chemical adsorption process rather than by the mass transfer process[20,57].
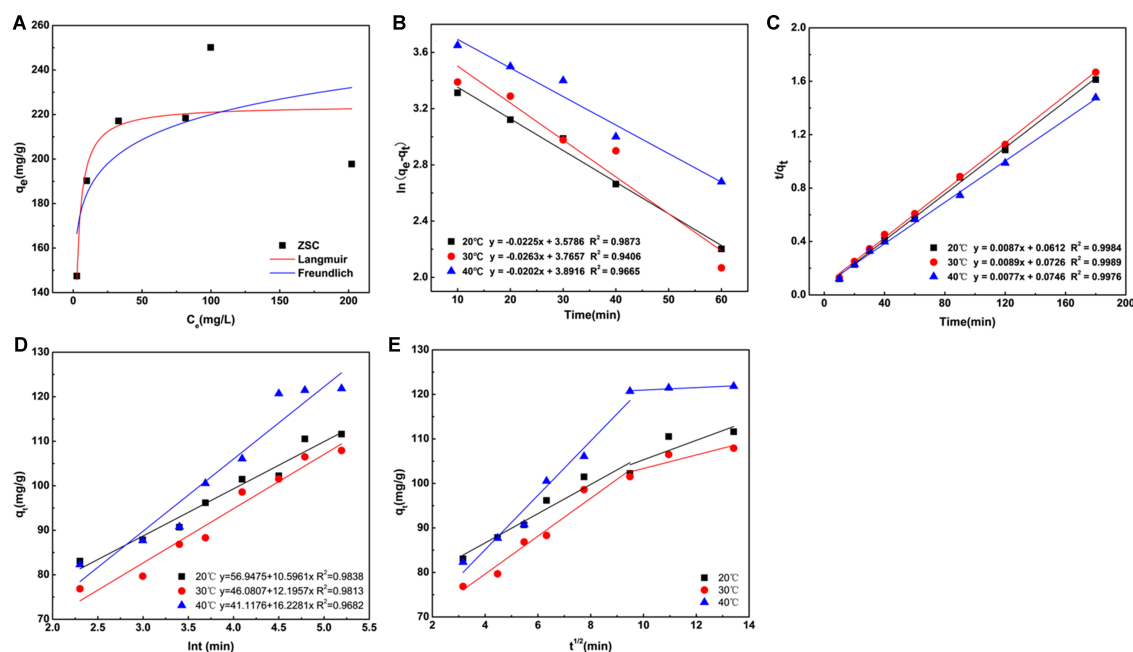
Figure 6. Adsorption isotherms. (A) Langmuir and Freundlich adsorption isotherms, and adsorption kinetic; (B) Pseudo-primary kinetics; and (C) Pseudo-secondary kinetics, (D) Elovich, (E) Intraparticle.

Adsorption summary

According to the literature research, the adsorption mechanism of organic substances by biochar predominantly included pore filling, hydrogen bonding, π-π interactions, electrostatic interactions, and complexation with oxygenated functional groups[58,59]. In this study, the adsorption behavior of ZSC on MG was explored by adsorption isotherms, adsorption kinetics, and experiments with different environmental factors. Results showed that the adsorption of MG by ZSC was notably in accordance with the pseudo-second kinetics and the Langmuir model. As such, the progression of the reaction was primarily ascribed to chemical factors, characterized by monolayer adsorption of individual molecules on a uniform surface, aligning with the results made by Gao *et al.*[21]. ZSC obtained a larger specific surface area and pore structure after pyrolytic carbonization, leading to increased surface active sites, which could be explained by the fact that higher temperature contributes to the decomposition and escape of volatiles, tars, and other products, leading to more microporous structures and larger specific surface area of biochar, and also affects the number of surface active sites of biochar[60]. Upon saturation of the surface active sites, MG slowly diffused into the pores, causing the low removal of MG. This result confirmed that the pore filling was involved in the adsorption process. Additionally, pyrolysis temperature could affect the order of formation of functional groups, and higher pyrolysis temperatures could increase the degree of aromatization of biochar[61]. The FT-IR results showed that ZSC contained functional groups such as –OH, C–O, and C=C, which were able to be attracted to form hydrogen bonding by the nitrogenous groups on the MG that were strongly negatively charged[62]. Moreover, oxygen-containing groups such as C–O were highly aromatized, which were hypothesized to be capable of π-π stacking[63], promoting efficient dye removal. As the pH increased, the acidic groups on the surface of biochar were ionized or dissociated, resulting in an increase in the negative surface charge and the enhancement of the electrostatic interaction of biochar[64], which was consistent with our results [Figure 4B]. The elevation of pH corresponded to a rise in the adsorption capacity of ZSC, suggesting that electrostatic interactions played a more significant role in the adsorption process. Overall, electrostatic interactions, pore filling, hydrogen bonding, and π-π interactions were responsible for the high MG removal in the ZSC adsorption process [Figure 7].
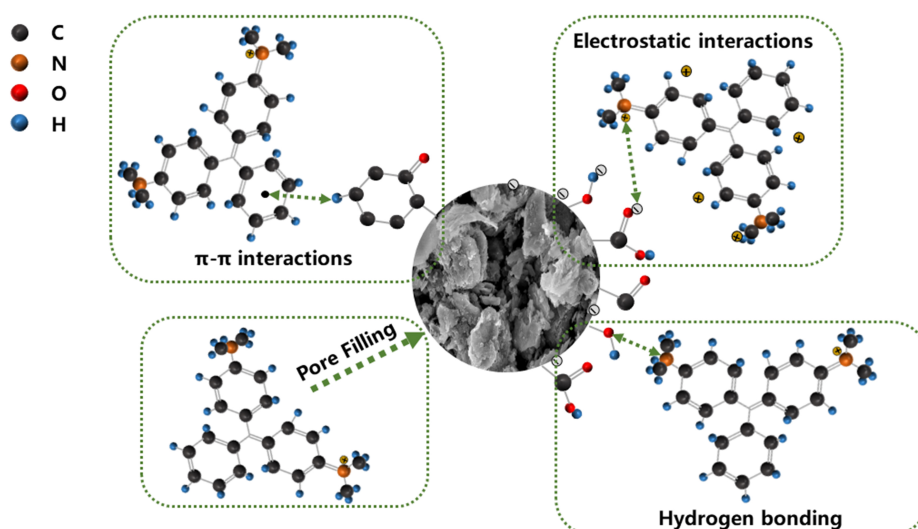
Figure 7. The adsorption mechanism of MG captured by ZSC. MG: malachite green; ZSC: ZnCl$_2$ modified sludge biochar.

CONCLUSION

In this study, a cost-effective dye adsorbent was successfully prepared from dyeing sludge. The combination of pyrolysis temperature, activation ratio, and carbonization time of 800 °C, 1:2 and 1.5 h, respectively, was found to be the optimal preparation conditions by response surface method, and the iodine adsorption value of ZSC was 340.99 mg/g. Meanwhile, the pyrolysis temperature was found to be the main factor affecting the pyrolysis process, followed by the activation ratio through the significance of each factor. The dyeing sludge biochar modified by ZnCl$_2$ activation had a better pore structure with a specific surface area of 495.38 cm^2/g. The adsorption equilibrium time, initial pH, initial MG concentration, ZSC dosage, and adsorption temperature would affect the removal of MG. Under the optimal conditions, the adsorption removal of MG by ZSC was as high as 99.13%. After five reuse cycles, ZSC could still adsorb 45% of MG. The adsorption performance conformed well to the Langmuir-type adsorption isotherm and pseudo-second kinetic model. In the ZSC adsorption process, electrostatic interactions, pore filling, hydrogen bonding, and π-π interactions could reflect the mechanism of high MG removal. In summary, employing sludge-derived activated carbon for the purification of organic wastewater could be a better choice for reducing and recovering sludge, while also proficiently processing dyeing wastewater.

DECLARATIONS

Authors' contributions

Conceptualization, methodology, data analysis: Qian W

Writing - original draft, investigation, data analysis: Deng Y

Investigation: Zhang Y

Data curation: Li Y

Visualization: Fang Y

Data curation, software: Li X

Writing - reviewing and editing, supervision: Liang J

Supervision, funding acquisition: Liu H

All authors listed have made a substantial, direct and intellectual contribution to the work and approved the final manuscript for publication.

REFERENCES

1. Xue G. Technology progress of dyeing wastewater treatment. *Ind Water Treat* 2021;41:10-7. DOI
2. Jia S, Huang MJ, Zhang B, Wei ZY, Cheng H, Li SZ. Research progress of biomass based carbon materials in the treatment of dyeing wastewater. *Chem Ind Forest Prod* 2023;43:145-56. DOI
3. Ou SF, Yang DS, Liao JW, Chen ST. Treating high COD dyeing wastewater via a regenerative sorption-oxidation process using a nano-pored activated carbon. *Int J Mol Sci* 2022;23:4752. DOI
4. Kolya H, Kang CW. Toxicity of metal oxides, dyes, and dissolved organic matter in water: implications for the environment and human health. *Toxics* 2024;12:111. DOI PubMed PMC
5. de Freitas LVP, Silveira JGF, Damaceno MA, et al. Evaluating the persistence of malachite green residues in tilapia and pacu fish. *Environ Toxicol Pharmacol* 2024;106:104382. DOI PubMed
6. Zahuri AA, Abdul Patah MF, Kamarulzaman Y, et al. Decolourisation of real industrial and synthetic textile dye wastewater using activated dolomite. *Water* 2023;15:1172. DOI
7. Dissanayake NSL, Pathirana MA, Wanasekara ND, Mahltig B, Nandasiri GK. Removal of methylene blue and Congo red using a chitosan-graphene oxide-electrosprayed functionalized polymeric nanofiber membrane. *Nanomaterials* 2023;13:1350. DOI PubMed PMC
8. Nguyen DDD, Phan Quang HH, Nguyen XH, Nguyen TP. The treatment of real dyeing wastewater by the electro-Fenton process using drinking water treatment sludge as a catalyst. *RSC Adv* 2021;11:27443-52. DOI PubMed PMC
9. Dong H, Liu H, Yang X, et al. The effect of initial conditions with aerobic biological treatment on aniline dyeing wastewater. *Processes* 2021;9:1329. DOI
10. Lin X, Zhou Q, Xu H, Chen H, Xue G. Advances from conventional to biochar enhanced biotreatment of dyeing wastewater: a critical review. *Sci Total Environ* 2024;907:167975. DOI PubMed
11. Deng D, Lamssali M, Aryal N, Ofori-Boadu A, Jha MK, Samuel RE. Textiles wastewater treatment technology: a review. *Water Environ Res* 2020;92:1805-10. DOI PubMed
12. Xue T, Shao F, Miao H, Li X. Porous polymer magnetic adsorbents for dye wastewater treatment. *Environ Sci Pollut Res Int* 2023;30:97147-59. DOI PubMed
13. He Y, Ni L, Gao Q, et al. Activated carbon with ultrahigh specific surface derived from bamboo shoot shell through K_2FeO_4 oxidative pyrolysis for adsorption of methylene blue. *Molecules* 2023;28:3410. DOI PubMed PMC
14. Castaldo R, Avolio R, Cocca M, Errico ME, Avella M, Gentile G. Amino-functionalized hyper-crosslinked resins for enhanced adsorption of carbon dioxide and polar dyes. *Chem Eng J* 2021;418:129463. DOI
15. Chen S, Tang S, Sun Y, et al. Preparation of a highly porous carbon material based on quinoa husk and its application for removal of dyes by adsorption. *Materials* 2018;11:1407. DOI PubMed PMC
16. Song J, Deng Q, Huang M, Kong Z. Carbon nanotube enhanced membrane distillation for salty and dyeing wastewater treatment by electrospinning technology. *Environ Res* 2022;204:111892. DOI PubMed
17. Boulanger N, Talyzin AV, Xiong S, Hultberg M, Grimm A. High surface area activated carbon prepared from wood-based spent mushroom substrate for supercapacitors and water treatment. *Colloid Surfaces A* 2024;680:132684. DOI
18. Lu J, Zhang Q, An Q, et al. Preparation of activated carbon from sewage sludge using green activator and its performance on dye

wastewater treatment. *Environ Technol* 2023;44:3897-910. DOI

19.   Li L, Ai J, Zhang W, et al. Relationship between the physicochemical properties of sludge-based carbons and the adsorption capacity of dissolved organic matter in advanced wastewater treatment: effects of chemical conditioning. *Chemosphere* 2020;243:125333. DOI PubMed

20.   Gong Y, Liu F, Liu H, Wang H, Zhao Y, Lin Y. Technology transition strategies for textile-dyeing sludge management in China from the environmental and economic perspectives. *Sustain Prod Consump* 2023;43:363-76. DOI

21.   Gao J, Zhou Y, Yang X, et al. Dyeing sludge-derived biochar for efficient removal of antibiotic from water. *Sci Total Environ* 2024;912:169035. DOI PubMed

22.   Fan Z, Zhou X, Peng Z, et al. Co-pyrolysis technology for enhancing the functionality of sewage sludge biochar and immobilizing heavy metals. *Chemosphere* 2023;317:137929. DOI PubMed

23.   Chen C, Sun J, Li Y, Zhao X, Wu H. Adsorption of methylene blue on activated carbon prepared from printing sludge. *Chin J Environ Eng* 2018;12:1872-8. Available from: http://eekw.rcees.ac.cn/en/article/doi/10.12030/j.cjee.201710068. [Last accessed on 24 Jul 2024]

24.   Wong S, Ngadi N, Inuwa IM, Hassan O. Recent advances in applications of activated carbon from biowaste for wastewater treatment: a short review. *J Clean Prod* 2018;175:361-75. DOI

25.   Zhang H, Wei Z, Xiong D, et al. Investigation into the structure and properties of biochar co-activated by $ZnCl_2$ and $NaHCO_3$ under low temperature conditions. *Materials* 2024;17:942. DOI PubMed PMC

26.   Oke N, Mohan S. Development of nanoporous textile sludge based adsorbent for the dye removal from industrial textile effluent. *J Hazard Mater* 2022;422:126864. DOI PubMed

27.   Wei S, Zhu M, Fan X, et al. Influence of pyrolysis temperature and feedstock on carbon fractions of biochar produced from pyrolysis of rice straw, pine wood, pig manure and sewage sludge. *Chemosphere* 2019;218:624-31. DOI PubMed

28.   Moško J, Pohořelý M, Skoblia S, et al. Structural and chemical changes of sludge derived pyrolysis char prepared under different process temperatures. *J Anal Appl Pyrol* 2021;156:105085. DOI

29.   Zou J, Yu J, Tang L, et al. Analysis of reaction pathways and catalytic sites on metal-free porous biochar for persulfate activation process. *Chemosphere* 2020;261:127747. DOI PubMed

30.   Wang RZ, Huang DL, Liu YG, et al. Recent advances in biochar-based catalysts: properties, applications and mechanisms for pollution remediation. *Chem Eng J* 2019;371:380-403. DOI

31.   Thue PS, Lima DR, Lima EC, et al. Comparative studies of physicochemical and adsorptive properties of biochar materials from biomass using different zinc salts as activating agents. *J Environ Chem Eng* 2022;10:107632. DOI

32.   Ferraro A, Marino E, Trancone G, et al. Assessment of environmental parameters effect on potentially toxic elements mobility in foreshore sediments to support marine-coastal contamination prediction. *Mar Pollut Bull* 2023;194:115338. DOI PubMed

33.   Wang X, Li C, Li Z, Yu G, Wang Y. Effect of pyrolysis temperature on characteristics, chemical speciation and risk evaluation of heavy metals in biochar derived from textile dyeing sludge. *Ecotoxicol Environ Saf* 2019;168:45-52. DOI PubMed

34.   Liang X, Ning X, Lin C, et al. Optimization of preparation conditions for activated carbons from textile dyeing sludge and sawdust using response surface methodology based on CCD. *Chin J Environ Eng* 2014;8:4937-42. Available from: http://hjhx.rcees.ac.cn/en/article/id/20141161?viewType=HTML. [Last accessed on 24 Jul 2024].

35.   Zhao WX, Zhou JY, Chen L, et al. Preparation and adsorption and catalytic performance of municipal sludge biochar. *Chem Res Appl* 2022;34:2531-7. Available from: https://cstj.cqvip.com/Qikan/Article/Detail?id=7108273947&from=Qikan_Search_Index. [Last accessed on 24 Jul 2024].

36.   Varela CF, Moreno-aldana L, Agámez-pertuz YY. Adsorption of pharmaceutical pollutants on $ZnCl_2$-activated biochar from corn cob: efficiency, selectivity and mechanism. *J Bioresour Bioprod* 2024;9:58-73. DOI

37.   Li Y, Chang F, Huang B, Song Y, Zhao H, Wang K. Activated carbon preparation from pyrolysis char of sewage sludge and its adsorption performance for organic compounds in sewage. *Fuel* 2020;266:117053. DOI

38.   Mahapatra U, Chatterjee A, Das C, Manna AK. Chemically activated carbon preparation from natural rubber biosludge for the study of characterization, kinetics and isotherms, thermodynamics, reusability during Cr(VI) and methylene blue adsorption. *Water Sci Technol* 2023;87:635-59. DOI PubMed

39.   Jian H, Yang F, Gao Y, et al. Efficient removal of pyrene by biochar supported iron oxide in heterogeneous Fenton-like reaction via radicals and high-valent iron-oxo species. *Sep Purif Technol* 2021;265:118518. DOI

40.   Chen J, Bai X, Yuan Y, Zhang Y, Sun J. Printing and dyeing sludge derived biochar for activation of peroxymonosulfate to remove aqueous organic pollutants: activation mechanisms and environmental safety assessment. *Chem Eng J* 2022;446:136942. DOI

41.   Zhai S, Li M, Wang D, Ju X, Fu S. Cyano and acylamino group modification for tannery sludge bio-char: enhancement of adsorption universality for dye pollutants. *J Environ Chem Eng* 2021;9:104939. DOI

42.   Li K, Lu H, Zhang Q, Li J. Adsorption of Cd(II) and Cu(II) onto clay modified with sludge activated carbon. *KSCE J Civ Eng* 2020;24:1706-16. DOI

43.   Wang B, Zhai Y, Wang T, et al. Fabrication of bean dreg-derived carbon with high adsorption for methylene blue: effect of hydrothermal pretreatment and pyrolysis process. *Bioresour Technol* 2019;274:525-32. DOI PubMed

44.   Xiao J, Wang L, Ran J, Zhao J, Tao M, Zhang W. Highly selective removal of cationic dyes from water by acid-base regulated anionic functionalized polyacrylonitrile fiber: fast adsorption, low detection limit, reusability. *React Funct Polym* 2020;146:104394. DOI

45.   Oladoye PO, Ajiboye TO, Wanyonyi WC, Omotola EO, Oladipo ME. Insights into remediation technology for malachite green wastewater treatment. *Water Sci Eng* 2023;16:261-70. DOI

46.   Maiti P, Mangsatabam M, Chatterjee A, Siddiqi H, Mishra A, Meikap B. In-situ synthesis of efficient $ZnCl_2$ doped pyrolyzed biochar

for adsorptive remediation of organic dyes: performance evaluation, mass transfer and mechanism. *Sep Purif Technol* 2024;329:125096. DOI

47.   Azim E, Samy M, Hanafy M, Mahanna H. Novel mint-stalks derived biochar for the adsorption of methylene blue dye: effect of operating parameters, adsorption mechanism, kinetics, isotherms, and thermodynamics. *J Environ Manage* 2024;357:120738. DOI PubMed

48.   Pirbazari A, Saberikhah E, Badrouh M, Emami MS. Alkali treated Foumanat tea waste as an efficient adsorbent for methylene blue adsorption from aqueous solution. *Water Res Ind* 2014;6:64-80. DOI

49.   Tang SH, Zaini MAA. Microporous activated carbon prepared from yarn processing sludge via composite chemical activation for excellent adsorptive removal of malachite green. *Surf Interfaces* 2021;22:100832. DOI

50.   Leng L, Yuan X, Huang H, et al. Bio-char derived from sewage sludge by liquefaction: characterization and application for dye adsorption. *Appl Surf Sci* 2015;346:223-31. DOI

51.   Zeng H, Qi W, Zhai L, Wang F, Zhang J, Li D. Magnetic biochar synthesized with waterworks sludge and sewage sludge and its potential for methylene blue removal. *J Environ Chem Eng* 2021;9:105951. DOI

52.   Raj A, Yadav A, Rawat AP, et al. Kinetic and thermodynamic investigations of sewage sludge biochar in removal of remazol brilliant blue R dye from aqueous solution and evaluation of residual dyes cytotoxicity. *Environ Technol Innov* 2021;23:101556. DOI

53.   Dai Q, Liu Q, Zhang X, et al. Synergetic effect of co-pyrolysis of sewage sludge and lignin on biochar production and adsorption of methylene blue. *Fuel* 2022;324:124587. DOI

54.   Li Y, Zhao M, Yan H, et al. Silica from rice husk for sludge-based biochar modification: as a novel adsorbent for lead. *J Water Process Eng* 2024;60:105218. DOI

55.   Zhao Z, Sun W, Ray MB. Adsorption isotherms and kinetics for the removal of algal organic matter by granular activated carbon. *Sci Total Environ* 2022;806:150885. DOI PubMed

56.   Li H, Kong J, Zhang H, et al. Mechanisms and adsorption capacities of ball milled biomass fly ash/biochar composites for the adsorption of methylene blue dye from aqueous solution. *J Water Process Eng* 2023;53:103713. DOI

57.   Chen Y, Li M, Li Y, et al. Hydroxyapatite modified sludge-based biochar for the adsorption of Cu^{2+} and Cd^{2+}: adsorption behavior and mechanisms. *Bioresour Technol* 2021;321:124413. DOI PubMed

58.   Gayathiri M, Pulingam T, Lee KT, Sudesh K. Activated carbon from biomass waste precursors: factors affecting production and adsorption mechanism. *Chemosphere* 2022;294:133764. DOI PubMed

59.   Qu J, Wang Y, Tian X, et al. KOH-activated porous biochar with high specific surface area for adsorptive removal of chromium (VI) and naphthalene from water: affecting factors, mechanisms and reusability exploration. *J Hazard Mater* 2021;401:123292. DOI

60.   Zhang W, Du W, Wang F, et al. Comparative study on Pb^{2+} removal from aqueous solutions using biochars derived from cow manure and its vermicompost. *Sci Total Environ* 2020;716:137108. DOI PubMed

61.   Liu C, Li H, Ni JQ, et al. Effect of municipal sludge-based biochar produced at different pyrolysis temperatures on humification and oxytetracycline degradation of pig manure composting. *Sci Total Environ* 2024;906:167816. DOI PubMed

62.   Zhao W, Zhao Y, Zhang H, Hao C, Zhao P. Efficient removal of cationic and anionic dyes by surfactant modified Fe_3O_4 nanoparticles. *Colloid Surfaces A* 2022;633:127680. DOI

63.   Wu JL, He H, Huang JY, Chen YR, Zhang WJ, Wang DS. Preparation of dyeing sludge-based carbon and its adsorption characteristics of dissolved organic matter in dredged residual water. *Saf Environ Eng* 2022;29:174-82. DOI

64.   Zeng Y, Lin Y, Ma M, Chen H. Adsorption effect and mechanism of Cd(II) by different phosphorus-enriched biochars. *Environ Sci Pollut Res Int* 2024;31:16642-52. DOI PubMed